Measuring Land-Surface Directional Reflectance with the Along-Track Scanning Radiometer

F.M. Danson, N.A. Higgins, and N.M. Trodd

Abstract

The Along-Track Scanning Radiometer (ATSR) was the first satellite-based instrument designed to routinely observe the Earth's surface at two different view zenith angles. ATSR-1, launched on ERS-1, was aimed specifically at measuring sea-surface temperature at high levels of precision; ATSR-2, launched on ERS-2, continued this mission but included three new channels in the visible and near infrared region which provided an opportunity to examine land-surface reflectance properties from nadir and near-coincident data from a sensor-view zenith angle of 55°. This paper examines the spectral and directional reflectance information in ATSR-1 and ATSR-2 data of a test site in southeastern Spain. Spectral variation is shown to account for approximately 76 percent of the total variance in the image data sets, with approximately 18 percent attributed to differences between the nadir and forward view images. Data quality issues are highlighted and issues concerned with collocation of the dual-view imagery are discussed.

Introduction

Most remote sensing instruments record images of the Earth's surface by making nadir or near-nadir measurements of the surface. These data are therefore a limited sample of the surface bidirectional reflectance distribution function (BRDF) which describes the anisotropic reflectance characteristics of the surface. However, it is well known that off-nadir measurements, which represent a different sample of the BRDF, contain additional information related to surface structure (Barnsley, 1994). The shape of the BRDF for vegetation canopies depends on a number of factors including leaf size and canopy architecture, but, in general, canopies exhibit higher reflectance in the backscatter direction (the "hot-spot") and lower reflectance in the forward scatter direction. Measurements of surface BRDF may therefore provide information on vegetation canopy properties that is not available in data sampled at nadir-view zenith angles.

A number of satellite-based instruments have a capability to make off-nadir measurements as a result of their wide field-of-view. The NOAA AVHRR, for example, makes measurements over a range of ±55° from nadir, perpendicular to the ground track of the satellite. Other instruments have an off-nadir pointing capability, like the SPOT-HRV which can be programmed to point to the side of the satellite at sensor view angles of up to 26°. These instruments provide the potential for increased sampling of the surface BRDF by utilizing the off-nadir viewing capability. However, a major limitation for quantitative analyses is that, although data for a given point on the Earth's surface may be obtained at different view angles, there is generally a time-lag of one or more days between the collection of spatially coincident measurements. This adds to the complexity of information extraction because of the differences in atmospheric conditions and solar position which may occur between images.

A new generation of imaging sensors designed specifically to sample the surface BRDF have been developed over the last ten years. These include the Airborne Solid-state Array Spectroradiometer (ASAS), which records data for a given area of the land surface at view angles from 55° forward of the aircraft to 55° behind the aircraft (Irons *et al.*, 1991); the POLDER (POLarization and Directionality of the Earth's Reflectance) instrument launched on the ADEOS satellite in 1996, which records data at 14 view angles (Deschamps *et al.*, 1994); and MISR (Multi-angle Imaging Spectro Radiometer), with nine view angles, to be launched on the first Earth Observing System in 1999 (Diner *et al.*, 1989).

The first operational satellite sensor to use forward-looking along-track scanning to obtain dual-view angle data was the Along Track Scanning Radiometer (ATSR-1), launched on the first European Remote Sensing satellite (ERS-1) in 1991. The ATSR-1 was designed to provide measurements of sea-surface temperature by using the dual-view angle data to derive an operational atmospheric correction exploiting the differences in path length between the forward and nadir views. The success of the ATSR-1 mission led to the design, build, and launch of ATSR-2 on ERS-2 in 1995. ATSR-2 provided additional wavebands in the visible and shortwave infrared region and offered the potential for extracting surface BRDF information over land surfaces (Barnsley *et al.*, 1994; Godsalve, 1996). This paper evaluates the potential of the ATSR instruments for land-surface applications, describes the results of experiments to investigate the spectral and directional reflectance properties of ATSR data, and identifies some of the issues for further development of off-nadir viewing sensors.

ATSR-1

The main goal of the ATSR-1 mission was to measure global sea-surface temperature (SST) with the high accuracy required by the climate change research community (Závody *et al.*, 1994; Závody *et al.*, 1995). The instrument has three thermal infrared channels (3.7μm, 10.8μm, and 12μm) and a single channel in the shortwave infrared (1.6μm) (Table 1). The 1.6-μm channel provides data for day time cloud screening and, as a late addition to the instrument, was not radiometrically calibrated (Wooster, 1996). Innovative features of ATSR-1 include precise on-board calibration of the thermal channels and an advanced detector cooling system, but, most notably, a novel inclined

Telford Institute of Environmental Systems, Department of Geography, University of Salford, Manchester M5 4WT, England.

Photogrammetric Engineering & Remote Sensing
Vol. 65, No. 12, December 1999, pp. 1411–1417.

0099-1112/99/6512–1411$3.00/0

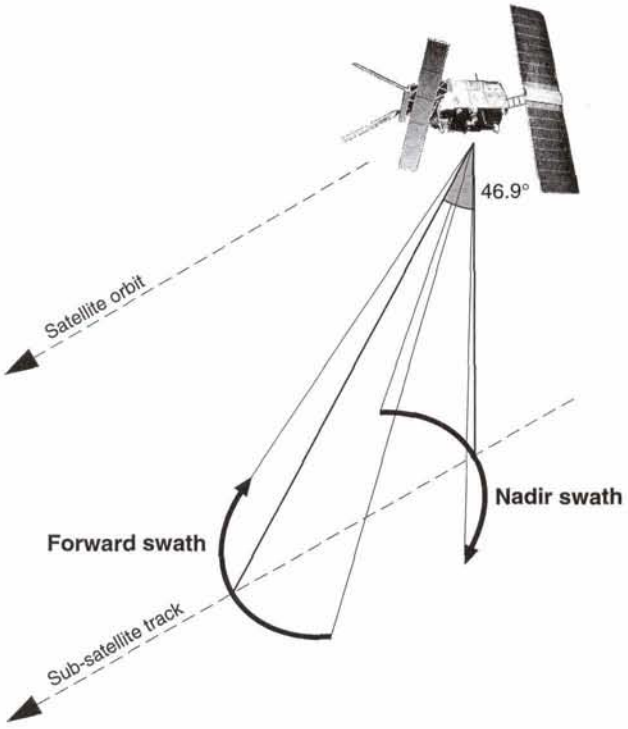

Figure 1. Conical scanning configuration of ATSR sensors.

conical scanning configuration (Figure 1). The sensor records a line of off-nadir pixels at a view zenith angle of approximately 55° and some 900 km along-track. Approximately 2 minutes later, a nadir view is obtained when the satellite is directly over the target. After resampling both the nadir and forward view data, the resultant image data set consists of two coregistered images with a 1-km spatial resolution and 512-km swath. These data allow accurate atmospheric correction over oceans by exploiting the information on atmospheric properties that may be derived from images of the same area collected within a few minutes of each other but through different atmospheric path lengths (Závody *et al.*, 1994; Godsalve, 1995). This dual-view angle capability, and accurate calibration, allows SST to be determined to accuracies of 0.3K or less (Závody *et al.*, 1995).

ATSR-2

The ATSR-2 was launched on ERS-2 in April 1995 to provide a continuation of the mission to measure global SST. It carried three additional channels in the visible and near infrared in order to provide measurements of land-surface reflectance properties (Table 1). However, the inclusion of these additional channels on ATSR-2 presented problems with the system data rate. ATSR-2 data are down linked at either high rate or low rate. In the high-rate mode, 12-bit data are available for all seven channels for all pixels in the swath. In operation, this mode is only available over land areas which are more than 800 km from a coastline. In oceanic and coastal areas, the ERS-2 Active Microwave Instrument is in routine operation, reducing the on-board memory available for ATSR data and necessitating the use of the low-rate data mode. Acquisition of data in the thermal channels is not compromised but, for the visible and SWIR channels, the low-rate mode means that data quality is reduced by discarded channels, data compression (12 bit to 10 or 8 bit), reduction in swath coverage, and interlacing (regular patterns of dropped pixels). In routine operation, low-rate data are collected for much of western Europe.

TABLE 1. SPECTRAL CHANNELS OF ATSR INSTRUMENTS

Channel	Center Wavelength (μm)	Bandwidth (μm)	ATSR-1	ATSR-2
V1 (green)	0.555	0.545 – 0.565		√
V2 (red)	0.659	0.649 – 0.669		√
V3 (near infrared)	0.865	0.855 – 0.875		√
1b (shortwave infrared)	1.61	1.58 – 1.64	√	√
1a (thermal infrared)	3.7	3.55 – 3.93	√	√
2 (thermal infrared)	10.85	10.4 – 11.3	√	√
3 (thermal infrared)	12.00	11.5 – 12.5	√	√

The ATSR-2 was operated successfully through to December 1995, although the scanning mechanism was known to be inferior to that of ATSR-1. This caused "scan jitter," which results in a significant loss of image data in the along-track direction. In December 1995 the instrument suffered a new problem with the scan mechanism, which led to the instrument being switched down. The system was restarted on 01 July 1996, but the data now suffer from severe scan jitter, which significantly reduces data quality.

Land Surface Applications of ATSR-1 and ATSR-2

The ATSR sensors offer a number of advantages over the NOAA AVHRR sensors which record data at similar spatial and spectral resolution. The ATSR sensors have a finer radiometric resolution, recording 12-bit data rather than the 10-bit of the AVHRR, and provide data in additional visible and shortwave infrared wavebands. These features combined with the dual-view angle capability have led to improved discrimination of clearings in dense tropical forest (Eva *et al.*, 1995) and the detection of thermal activity in volcanic lava domes using ATSR-1 channel 1b data (Wooster and Rothery, 1997). Other studies have examined the structure of ATSR-2 data over a number of different forest and grassland sites and showed, using principal components analysis, that the dual-view angle data contained information that was not present in the nadir view data alone (Gemmell and Millington, 1997; Perrin and Millington, 1997).

Angular and Spatial Sampling Characteristics of ATSR Instruments

The dual-view angle capability of the ATSR instruments provides new opportunities to examine the BRDF of land surfaces but also presents new challenges for data correction and interpretation. In contrast to ocean areas, the land surface is highly heterogeneous in terms of land-cover type and BRDF. This presents problems for atmospheric correction and data interpretation because, at the image scale, differences in the dual-view angle data are caused by a combination of atmospheric effects and surface BRDF effects. At the pixel scale, interpretation problems arise in areas of heterogeneous land cover because of the differences in the size and location of the forward and nadir ground resolution elements (GRE) (Godsalve, 1996).

The size of the GRE in the nadir view image is 1 km at the sub-satellite point, but, in the forward view, the GRE is irregular and approximately 1.5 by 2 km in size. The GRE size increases away from the sub-satellite track in both the forward and nadir view, with the largest elements at the edges of the forward view scan lines. These data are geolocated and collocated using navigation software which models the conical scanning mechanism, the satellite orbit and attitude control, and the shape and rotation of the Earth (Bailey, 1995; Godsalve, 1996). The standard 512- by 512-pixel 1-km gridded product is produced by nearest-neighbor sampling of the original ungridded data. However, due to the under sampling of the forward view (only 371 pixels to fill 512 gridded pixels across-track) a large number of the forward image pixels remain unfilled. There are 555

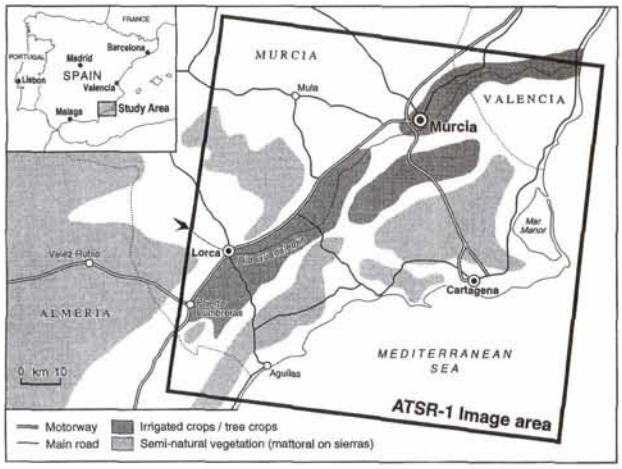

Figure 2. Study area.

pixels across track in the nadir view, but a small number also remain unfilled. Unfilled pixels are cosmetically filled by copying the spatially nearest of their eight neighbors (Bailey, 1995).

As a result of the angular sampling and resampling procedure, there is considerable uncertainty in the collocation of the forward and nadir view pixels. Each 1-km nadir-view pixel has a collocated forward-view pixel which is derived from an irregular GRE of at least 1.5 by 2 km, which is derived by nearest-neighbor resampling and which may be cosmetically filled. A major problem therefore in interpreting ATSR data is that, unless the land surface is homogeneous over the area of the forward view GRE, or the forward and nadir GRE contain a similar mix of land-cover types and therefore BRDF, the dual-view data are samples of different surface BRDF. As a consequence, it is likely to be very difficult to combine the information from the forward and nadir views on a pixel-by-pixel basis (Prata *et al.*, 1990).

The dual-view angle capability of the ATSR sensors provides data at two different view zenith angles, but seasonal variation in the solar position means that, like all remotely sensed data, the solar azimuth angle changes from image to image. In the southern hemisphere, the ATSR instruments record forward-view images in the backscatter direction, and the reflectance recorded over vegetated surfaces would be expected to be higher than in the nadir view. In the northern hemisphere, the forward-view data are from the forward scatter direction where reflectance should be lower than in the nadir view. However, the 1030 hours equatorial crossing time and the orbital inclination of 98.2° of the ERS platforms means that the forward-view direction is never close to the principal plane (relative azimuth is 0° or 180°) so that reflectance differences between the nadir and forward-view images may be smaller than expected.

Comparison of ATSR-1 and ATSR-2 Data

ATSR-1 and ATSR-2 data were acquired for a test area in the Murcia Province of southeastern Spain (Figure 2). An ATSR-1 image was obtained for 04 May 1994 and an ATSR-2 image for 19 May 1995, close to the date of a field data collection campaign which took place in April 1995. These data sets are currently being used in a number of studies to examine the land-cover information in ATSR data. The focus of this paper is to evaluate the spectral and directional information in the data sets and to outline issues associated with data quality and data interpretation.

ATSR-1 Data

A 100- by 100-km sub-scene was extracted from the original 512- by 512-km image to correspond to the study area and also effectively reduce the within-image variation in solar illumination and sensor view angles. There is still some variation in the illumination and viewing conditions within the scene (Table 2), with a range in the sensor-view zenith angle in the nadir image of 9.5° to 18.1° and a range in the relative azimuth angle between the illumination and view directions in the nadir image of 153.4° to 162.9°. The ranges for the full scene are much larger, with the relative azimuth angle varying between 25.5° and 61.8°, a variation of 36° (Table 2). It is clear from these data that the variation in illumination and viewing geometry varies significantly across any ATSR-1 image. This has implications for data interpretation because every pixel in the image represents a different sample of the BRDF of the surface. The variations for the sub-scene were smaller however and, for the purposes of this paper, were assumed to have a relatively small impact on the spatial variation in the image data.

Because we are concerned mainly with reflected radiation, the data analysis was restricted to the uncalibrated Channel 1b data in the shortwave infrared, which were processed as nadir and forward-view 1-km gridded images (Figure 3). The nadir image shows clearly the spectral contrast between the land and sea and between areas of semi-natural mattoral vegetation, which is dark, and the agricultural areas, which have lighter tone in the image. This spectral variation is also evident in the forward-view image, although the spectral contrast is smaller and the image appears smoothed because of the larger GRE of the sensor in the forward view.

To examine the spectral and directional information content of the image, a random sample of 1000 pixels was extracted and plotted in dual-view angle feature space (Figure 4). Pixels which have the same digital number (DN) in the forward and nadir view are located on the 1:1 line; pixels which have different DN at the two views are located above or below that line. Two main clusters of pixels may be identified: the first, with low DN at both views, corresponds to the Mediterranean sea and the second, with pixels below the 1:1 line, corresponds to the land surface. The sea pixels generally have a higher forward-view DN because of the additive effect of path radiance, which is important over dark targets. Pixels over land have a lower DN in the forward view, indicating that the surface has a lower

TABLE 2. RANGE IN SOLAR ILLUMINATION AND SENSOR VIEW ANGLES FOR ATSR-1 IMAGE

		Full Scene 512 by 512 km		Sub-scene 100 by 100 km	
		Minimum	Maximum	Minimum	Maximum
Nadir Image	Solar Zenith Angle	22.4	26.2	22.9	23.9
	View Zenith Angle	0.5	22.2	9.5	18.1
	Relative Azimuth Angle	122.2	167.6	153.4	162.9
Forward Image	Solar Zenith Angle	23.7	27.5	23.8	24.2
	View Zenith Angle	52.6	55.4	53.7	55.0
	Relative Azimuth Angle	25.5	61.8	29.0	36.1

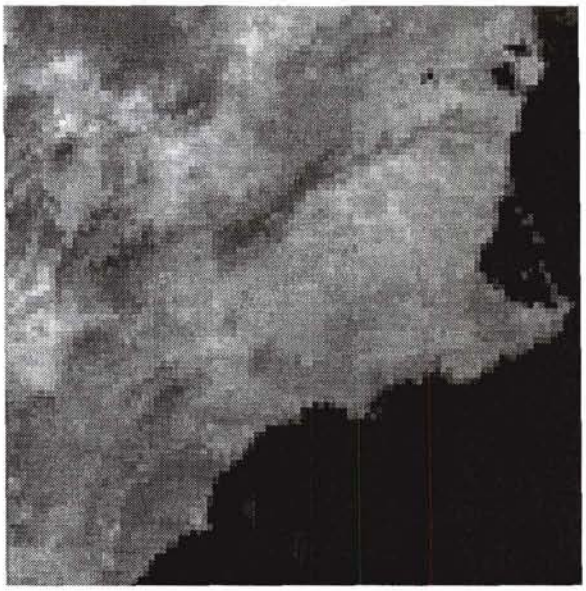

NADIR VIEW

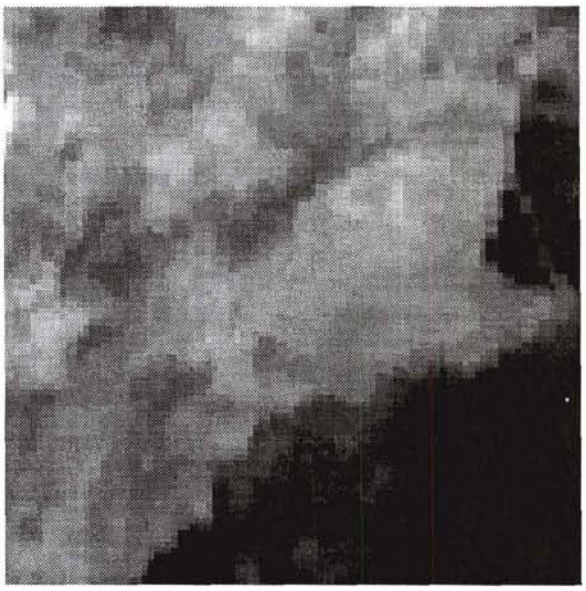

FORWARD VIEW

Figure 3. ATSR-1 gridded 1-km nadir and forward-view image of southeastern Spain, Channel 1b, 04 May 1994.

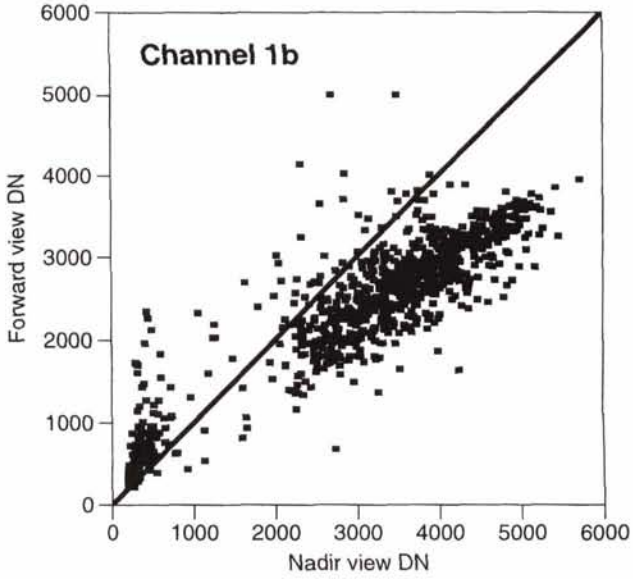

Figure 4. ATSR-1 Channel 1b dual-view angle data space.

reflectance at the forward view. The effects of path radiance may be relatively small over the land, which has intermediate levels of reflectance, and the BRDF differences are the key controlling factor. The linear correlation between the DN at the two views was 0.9, showing that, although there is a clear difference in the DN, they are highly correlated so that the directional information content of the scene as a whole is low.

To visualize the spatial variation in directional reflectance, forward view DN (DN_f) and nadir view DN (DN_n) were combined as the Directional Reflectance Index (DRI): i.e.,

$$DRI = (DN_f/DN_n). \quad (1)$$

The DN in the DRI image (Figure 5) represent isolines in the dual-view angle feature space which converge at the origin. For clarity, the image grey scale has been reversed so that pixels with a DRI of one or greater appear black, and lower ratios are represented by brighter tones. The image shows clearly the difference between land and sea, and the small inland lagoons at the top left of the image are also clearly defined. The lowest ratios (brightest tone) occur along the coast, but there is relatively little variation in the DRI over much of the land surface. The dark areas at the top left of the image are cloud. The DRI image confirms the observation made previously that BRDF dif-

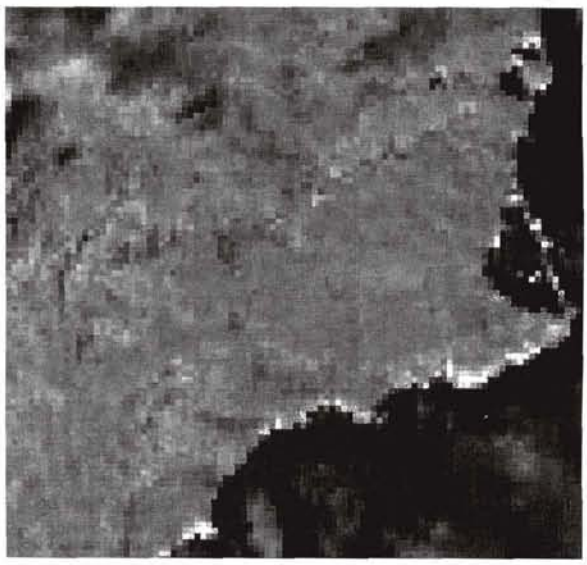

Figure 5. Directional Reflectance Index image for ATSR-1 Channel 1b data.

TABLE 3. RANGE IN SOLAR ILLUMINATION AND SENSOR VIEW ANGLES FOR ATSR-2 IMAGE

		Full Scene 512 by 512 km		Sub-Scene 84 by 84 km	
		Minimum	Maximum	Minimum	Maximum
Nadir Image	Solar Zenith Angle	19.5	26.1	22.8	23.5
	View Zenith Angle	0.6	22.2	2.6	8.7
	Relative Azimuth Angle	7.6	142.9	111.5	139.6
Forward Image	Solar Zenith Angle	19.7	26.0	23.1	23.8
	View Zenith Angle	51.8	54.5	54.1	54.5
	Relative Azimuth Angle	31.2	81.0	59.9	65.7

ferences are large between land and water, but that differences caused by land-cover variation are small.

ATSR-2 Data

A smaller 84- by 84-km sub-scene was extracted in order to examine the directional reflectance of the ATSR-2 image. This again reduced the intra-image illumination and view-angle variation (Table 3) and allowed the data analysis to focus on variation in directional reflectance. As a preliminary stage, the data for all available visible and SWIR channels were displayed as collocated 1-km gridded nadir and forward views (Figure 6). This showed a number of significant data quality problems:

- Channel V1 was not recorded in the forward view;
- Interlacing was evident in channels V1, V2, and V3;
- Scan jitter caused extensive data loss in the along-track direction in channels V1, V2, and V3;
- The "peppered" appearance of the data in some channels showed the extent of pixels which would be cosmetically filled at the next level of data processing;
- Although not evident in Figure 6, channels V2 and V3 were recorded as 8-bit data rather than the full 12-bit quantization.

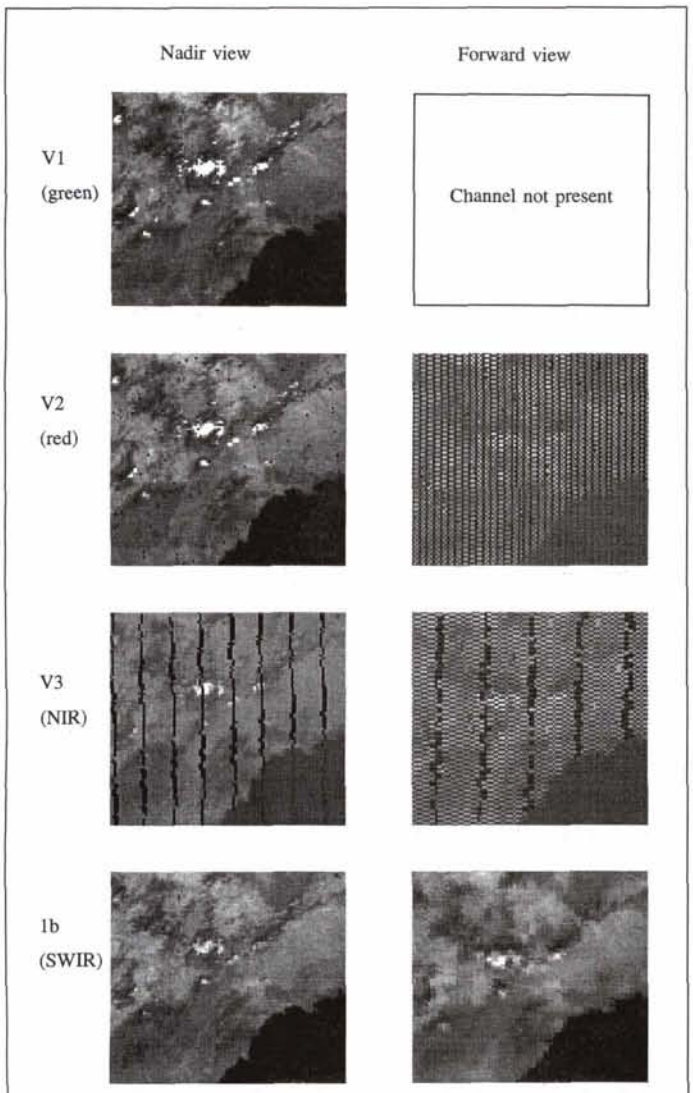

Figure 6. ATSR-2 data for southeastern Spain, 19 May 1995.

These problems result from the use of low-rate data collection over southeastern Spain, but, fortunately, it was possible to identify only those pixels which were unaffected by interlacing, scan jitter, or cosmetic copying, and the data analysis proceeded with these pixels. No attempt was made to produce DRI images, but 1000 pixels were extracted to examine the information content in dual-view angle data space.

As a preliminary stage, the data were radiometrically calibrated to top-of-the-atmosphere reflectance using calibration data supplied by the Rutherford Appleton Laboratory. The forward- and nadir-view data were then atmospherically corrected using the 6S model of Vermote *et al.* (1997). 6S input variables may be selected from models of standard atmospheres or else defined by the user. The input variables include geometrical conditions, aerosol, water, ozone concentration, and target elevation. For each view, top-of-atmosphere reflectance was determined in channel V2 for the pixel with the lowest value over an area of deep clear water. The aerosol optical scattering parameters were assumed to be those of a continental aerosol model, and the estimates of aerosol optical depth at 550 nm derived from 6S were 0.19 for the nadir image and 0.20 for the forward-view image. A typical midlatitude summer atmospheric profile was assumed for water and ozone concentration (Vermote *et al.*, 1997), and the elevation for each pixel was derived from a co-registered elevation model. In the method used here, a Lambertian surface reflectance was assumed. The application of 6S enabled correction of the effects of atmospheric scattering and absorption on the ATSR-2 data but, most importantly, accounted for path length differences between the forward and nadir view.

Plots of the data in dual-view angle data space revealed patterns very similar to those observed in data for the same area for the previous year using ATSR-1 data (Figure 7). Most pixels had a higher reflectance in the nadir view, with the exception of a small number of sea pixels, and land/sea boundary pixels which had a higher reflectance in the forward view. Because the effect of differences in atmospheric path length between the nadir and forward-view data had been corrected, the deviation of a given pixel from the 1:1 line for a given spectral channel can be interpreted as a difference in directional reflectance between the two views. The data indicate that, in an area composed of a mix of semi-natural vegetation and agriculture, the surface directional reflectance is significantly higher in the nadir view than in the forward view. This conclusion is, of

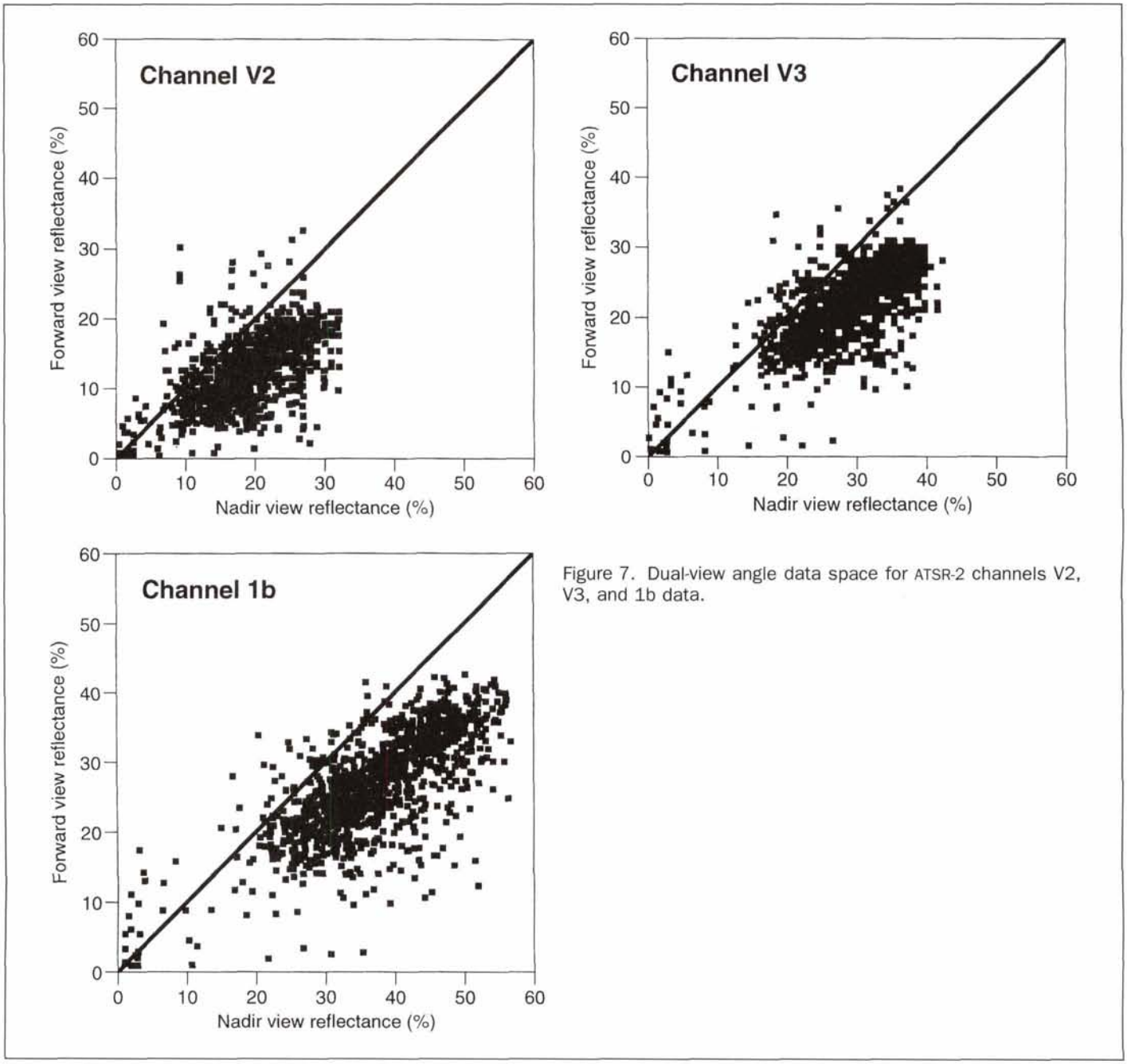

Figure 7. Dual-view angle data space for ATSR-2 channels V2, V3, and 1b data.

course, only valid for the illumination and viewing conditions under which the data were collected.

Principal Components Analysis

Principal components analysis was used to examine the statistical structure of the data over the study area. Pixels containing water were first removed by reference to a Landsat TM scene, and a principal components analysis was performed using the data for channels V2, V3, and 1b for both forward and nadir views. The results (Table 4) showed that approximately 76 percent of the variance in the combined data set was explained by the first principal component. This corresponds to the "brightness" dimension commonly observed in nadir-view data and is represented by the main axis of the dual-view angle data space (Figure 7). The second principal component accounted for a further 18 percent of the variation and is related to the contrast in reflectance between the forward- and nadir-view data. The third and fourth principal components accounted for 5 percent of the variation and represent contrasts between channel 1b and channels V3 and V2, respectively. The fifth principal component was weakly related to channel V2 but accounted for only 0.6 percent of the variation. A small residual level of variation, allocated to the sixth principal component, may be con-

TABLE 4. PRINCIPAL COMPONENTS ANALYSIS OF DUAL-VIEW ANGLE ATSR-2 DATA

Eigenvector	Eigenvalue	Variance (%)	Interpretation
1	4.541	75.7	Spectral
2	1.072	17.9	Directional
3	0.214	3.6	Spectral
4	0.098	1.6	Spectral
5	0.038	0.6	Spectral
6	0.036	0.6	Noise

TABLE 5. EIGENVECTOR LOADINGS FOR DUAL-VIEW-ANGLE ATSR-2 IMAGE

View	Channel	Eigenvector 1	2	3	4	5	6
Nadir	V2	0.868	−0.444	−0.036	0.194	0.100	0.008
Nadir	V3	0.872	−0.399	0.254	0.046	0.069	0.092
Nadir	1b	0.873	−0.415	−0.193	−0.131	0.052	0.095
Forward	V2	0.848	0.487	−0.069	0.162	0.113	0.010
Forward	V3	0.856	0.430	0.256	−0.066	−0.064	0.086
Forward	1b	0.901	0.349	−0.203	−0.106	−0.065	−0.102

sidered to represent scene noise. This interpretation is reinforced by examining the eigenvector weightings for each channel (Table 5). There were high positive loadings for all six channels on the first principal component, showing the spectral brightness response. The third, fourth, and fifth principal components also accounted for variation associated with spectral characteristics of the data, such that 81 percent of the total variance was related to spectral variation. Only the second principal component clearly showed contrast between loadings on the forward- and nadir-view channels. The principal components analysis reinforces the conclusion that the main variation in ATSR-2 dual-view angle data is related to spectral variation but that a second significant variation of around 18 percent may be attributed to the angular sampling of the instrument. Again, this conclusion is only valid for this environment and measurement conditions and may be different with the inclusion of channel V1 data.

Conclusions

The work presented in this paper illustrates both the potential and the problems associated wth measuring land-surface directional reflectance using the ATSR sensors. It is clear that the dual-view angle data sets provided by ATSR-1 and ATSR-2 provide information on surface BRDF, and the implication for using these dual-view angle data is that users may have access to 18 percent more information than would be available in nadir-view data sets. However, the spatial sampling differences between the two views presents a significant challenge for measuring BRDF in areas of heterogeneous land cover.

Data quality problems with the ATSR-2 visible channels are partly due to the data rate limitations and partly to mechanical malfunction. It is important that high quality visible data are acquired for the whole of the Earth's land surface, and it is anticipated that this will be possible with the Advanced Along-Track Scanning Radiometer (AATSR) which will be launched on the European Space Agency's Envisat in 1999. The AATSR is funded primarily by the UK in order to provide a complete continuous ten-year record of global SST. The instrument is identical to its predecessors but has a number of additional features, including on-board calibration of the visible and SWIR channels using the Sun as a reference, and, unlike ATSR-2, will have no data-rate limitations, recording full 16-bit digitization at all times.

The next five years will see the launch of a number of off-nadir viewing sensors designed to obtain information on land-surface BRDF. Data from the ATSR-1 and ATSR-2 have shown the important contribution that will be made by these sensors to understanding land-surface reflectance properties and have also highlighted areas which require further investigation.

Acknowledgments

The authors acknowledge the support of the British Council and Manchester Geographical Society. NAH was supported by a Natural Environment Research Council research studentship GT12/94/EOP/18.

References

Bailey, P., 1995. *Sadist-2 v100 Products*, Space Science Department, Rutherford Appleton Laboratory, UK, 25 p.

Barnsley, M.J., A.H., Strahler, K.P. Morris, and J.-P Muller, 1994. Sampling the surface bidirectional reflectance distribution function (BRDF): Evaluation of current and future satellite sensors, *Remote Sensing Reviews*, 8:271–311.

Deschamps, P.Y., F.M. Bréon, M. Leroy, A. Podaire, A. Bricaud, J.C. Burriez, and G. Sèze, 1994. The POLDER Mission: Instrument characteristics and scientific objectives, *IEEE Transactions on Geoscience and Remote Sensing*, 32:598–615.

Diner, D.J., C.J. Bruegge, J.V. Martonchik, T.P. Ackerman, R. Davies, S.A.W. Gerstl, H. R. Gordon, P.J. Sellers, J. Clark, J.A. Daniels, E.D. Danielson, D.I. Nakamoto, R. Pagano, and T.H. Reilly, 1989. MISR: A Multiangle SpectroRadiometer for geophysical and climatological research from EOS, *IEEE Transactions on Geoscience and Remote Sensing*, 27:200–214.

Eva, H.D., G. D'Souza, and J.P. Maligreau, 1995. Potential of ATSR-1 for detection of clearings within dense humid tropical forest, *International Journal of Remote Sensing*, 16:2071–2079.

Gemmell, F.M., and A.C. Millington, 1997. Initial assessment of ATSR-2 data structure for land surface applications, *International Journal of Remote Sensing*, 18:461–466.

Godsalve, C., 1995. Bidirectional reflectance sampling by ATSR-2: A combined orbit and scan model, *International Journal of Remote Sensing*, 16:269–300.

———, 1996. Simulation of ATSR-2 optical data and estimates of land surface reflectance using simple atmospheric corrections, *IEEE Transactions on Geoscience and Remote Sensing*, 34:1204–1212.

Higgins, N.A., F.M. Danson, and N.M. Trodd, 1996. Modelling vegetation spectral response at ATSR-2 view angles, *Remote Sensing Science and Industry*, Remote Sensing Society, Nottingham, pp. 543–548.

———, 1997. Effects of vegetation structure on canopy directional reflectance spectra, *Physical Measurements and Signatures in Remote Sensing*, G. Guyot and T. Phulpin, (editors), Balkema, Rotterdam, pp. 275–280.

Irons, J.R., K.J. Ranson, D.L. Williams, R.R. Irish, and F.G. Heugel, 1991. An off-nadir imaging spectroradiometer for terrestrial ecosystem studies, *IEEE Transactions on Geoscience and Remote Sensing*, 29:66–74.

Perrin, M.C., and A.C. Millington, 1997. ATSR-2 data for burned area detection, *Observations and Interactions*, Remote Sensing Society, Nottingham, pp. 165–170.

Prata, F.A.J., R.P. Cechet, I.J. Barton, and D.T. Llewellyn-Jones, 1990. The Along Track Scanning Radiometer for ERS-1 - Scan geometry and data simulation, *IEEE Transactions on Geoscience and Remote Sensing*, 28:3–13.

Vermote, E.F., D. Tanré, J.L. Deuzé, M. Herman, and J.J. Morcrette, 1997. Second simulation of the satellite signal in the solar spectrum: An overview, *IEEE Transactions on Geoscience and Remote Sensing*, 35:675–686.

Wooster, M.J., 1996. In-orbit calibration of the ATSR-1 1.6μm channel using high resolution data from the JERS-1 (Fuyo-1) optical sensor, *International Journal of Remote Sensing*, 17:1069–1074.

Wooster, M.J., and D.A. Rothery, 1997. Thermal monitoring of Lascar Volcano, northern Chile, using infrared data at high temporal resolution: A 1992 to 1995 time series using the Along Track Scanning Radiometer, *Bulletin of Volcanology*, 58:566–579.

Závody, A.M., M.R. Gorman, D.J. Lee, D. Eccles, C.T. Mutlow, and D.T. Llewellyn-Jones, 1994. The ATSR data processing scheme developed for the EODC, *International Journal of Remote Sensing*, 15:827–843.

Závody, A.M., C.T. Mutlow, and D.T. Llewellyn-Jones, 1995. A radiative transfer model for sea surface temperature retrieval for the along-track scanning radiometer, *Journal of Geophysical Research*, 100:937–952.

(Received 22 July 1998; accepted 03 November 1998; revised 07 January 1999)